2025 IEEE/SICE International Symposium on System Integration (SII)
January 21-24, 2025, Munich, Germany

Development of Unmanned Surface Vehicle "i-Boat2" for Inspection of Underside of Pier and Its Autonomous Navigation Experiments

Sunao Nakamaru[1], Yuma Yabuki[1], Aki Yokoyama[1], Naoyuki Takesue[1]
Kenichi Mizuno[2], Takahiro Sakai[2] and Osamu Taniguchi[2]

***Abstract*— The number of port facilities in Japan that were constructed more than 50 years ago is rapidly increasing. Therefore, it is necessary to take measures to ensure the safety and maintain the functionality of the facilities. However, in conventional inspections, inspectors board a boat and use a camera to take pictures of cracks, peeling and other defects on the wall surface to analyze the degree of deterioration, which requires a huge amount of time and money. Therefore, in this study, we have developed an unmanned surface vehicle for efficient inspection of the underside of piers. This paper proposes a sway suppression control and a path following control, and reports the results of autonomous navigation experiments using the robot in a real ocean environment.**

I. Introduction

The number of port facilities in Japan that were constructed more than 50 years ago is rapidly increasing. Therefore, it is necessary to take measures to ensure the safety and maintain the functionality of the facilities [1].

However, in conventional inspections of port facilities, inspectors board a boat and use a camera to take pictures of defective areas such as cracks, peeling and others on the wall surface, or make a sketch drawing before analyzing the degree of deterioration [2], [3], which requires a huge amount of time and money. Periodic inspection and diagnosis are required to efficiently and early detect the occurrence and progression of deformations (abnormalities on the surface of concrete due to damage, deterioration, or other causes). However, the inability of many local governments to conduct inspections and diagnostics, and the limited financial and human resources available for these activities, make more efficient maintenance and management of port facilities a challenge.

Recently, ship-based unmanned surface vehicles (USVs) have been developed [4]–[8], but they are too large to perform inspections under piers. On the other hand, underwater drones are easy to use under piers, but because they cannot receive radio waves, they must use cables and there is a risk of cable entanglement [9], [10].

Therefore, an inspection method using a radio-controlled boat equipped with a camera ("i-Boat" shown in Fig. 1) was developed for efficient inspection of port facilities [2], [3]. Although this method is more efficient than the conventional inspection method in which inspectors board a boat, it requires skill to maneuver the boat through the camera view, and autonomous navigation is desired as an easier and more efficient method of operation. Therefore, this research aims to develop a USV, "i-Boat2", that can navigate autonomously and stably under dynamic disturbances and in environments where global navigation satellite system (GNSS) is difficult to use. This paper presents the development of i-Boat2, which is a USV equipped with four thrusters, 3D light detection and ranging (LiDAR) and inertial measurement unit (IMU), proposes a sway suppression control and path following control, and conducts autonomous navigation experiments at a real port facility. Using the methods in this study, autonomous navigation using SLAM would be possible even for small, lightweight vessels that are easily swept away by waves.

Fig. 1. Radio-controlled boat "i-Boat" [2], [3]

Fig. 2. Unmanned surface vehicle "i-Boat2"

II. Unmanned Surface Vehicle i-Boat2

A. System Configuration

The appearance of the USV "i-Boat2" developed in this study is shown in Fig. 2, and its configuration is shown in Fig. 3. The i-Boat2 is a boat that can move in all directions by means of four symmetrically arranged thrusters, which is called "X" type in [11]. The boat is made of fiber reinforced plastic (FRP) and measures 1.2 m in length, 0.8 m in width, and 0.64 m in height, with a total weight of 53 kg.

[1]Sunao Nakamaru, Yuma Yabuki, Aki Yokoyama and Naoyuki Takesue are with Tokyo Metropolitan University, Hino-shi, Tokyo, Japan. [2]Kenichi Mizuno, Takahiro Sakai and Osamu Taniguchi are with Penta-Ocean Construction Co., Ltd.

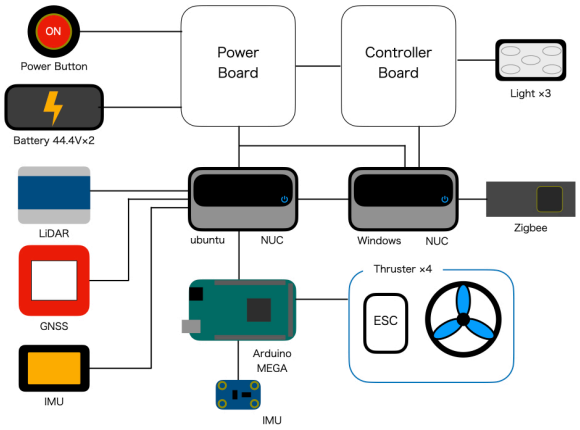

Fig. 3. System configuration

TABLE I

MAIN COMPONENTS OF I-BOAT2

Component	Product (Manufacturer)
PC	NUC (Intel)
3D LiDAR	VLP-16 (Velodyne)
IMU	3DM GX5-AHRS (MicroStrain) BNO055 (Bosch)
Microcontroller	M5Stack Basic (M5Stack)
GNSS	ZED-F9P (u-blox)
Thruster	T200 (Blue Robotics)

Two PCs for higher-level control and communication and a microcontroller for lower-level control are installed on this boat, and simultaneous localization and mapping (SLAM) with 3D LiDAR and IMU is used for autonomous navigation. The main components are listed in Table I.

B. Thruster Control

Figure 4 shows the thruster arrangement of i-Boat2 when the positive X-axis is in front and the positive Y-axis is to the left as a coordinate system. Only the left side of robot is shown in the figure because it is symmetrical. With the robot centered at the origin O, the position of the thruster attached to the left front side is (r_{1x}, r_{1y}) and the position of the thruster attached to the left rear side is $(-r_{2x}, r_{2y})$. Let $\boldsymbol{f}_R = [f_x,\ f_y,\ m_z]^{\mathrm{T}}$ be the propulsive force (forward/backward, left/right, and rotation) of the robot, the relationship to the thrust of the four thrusters $\boldsymbol{f}_T = [f_1,\ f_2,\ f_3,\ f_4]^{\mathrm{T}}$ can be expressed as follows:

$$\boldsymbol{f}_R = \boldsymbol{A}\,\boldsymbol{f}_T \tag{1}$$

where

$$\boldsymbol{A} = \frac{\sqrt{2}}{2}\begin{bmatrix} 1 & -1 & -(r_{1x}+r_{1y}) \\ 1 & 1 & -(r_{2x}+r_{2y}) \\ 1 & -1 & r_{2x}+r_{2y} \\ 1 & 1 & r_{1x}+r_{1y} \end{bmatrix}^{\mathrm{T}} \tag{2}$$

The pseudo-inverse of $\boldsymbol{A}$ is used to obtain the thruster thrust $\boldsymbol{f}_T$ from the robot thrust $\boldsymbol{f}_R$ as follows:

$$\boldsymbol{f}_T = \boldsymbol{A}^{+}\,\boldsymbol{f}_R \tag{3}$$

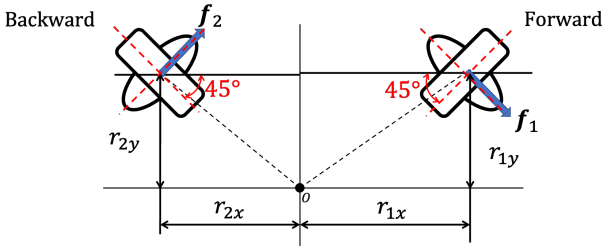

Fig. 4. Thruster arrangement

where

$$\boldsymbol{A}^{+} = \frac{\sqrt{2}}{2r_s}\begin{bmatrix} r_s/2 & -(r_{2x}+r_{2y}) & -1 \\ r_s/2 & r_{1x}+r_{1y} & -1 \\ r_s/2 & -(r_{1x}+r_{1y}) & 1 \\ r_s/2 & r_{2x}+r_{2y} & 1 \end{bmatrix} \tag{4}$$

$$r_s = r_{1x} + r_{1y} + r_{2x} + r_{2y} \tag{5}$$

C. Sway Suppression Control

The environment is subject to wind and waves, which can cause the robot to sway. Compared to a vessel such as the i-Boat2, a small and light boat is easily swept away by waves. Therefore, feedback with SLAM and sway control for waves are used. This sway can affect the stability and accuracy of SLAM. The robot has four thrusters, so it is not possible to control the translational motion and the rotational motion independently. However, the following control is considered to suppress the sway.

Let ω_r, ω_p and ω_y be the angular velocities of the robot around the roll (x), pitch (y) and yaw (z) axes as measured by the IMU. In this case, the thrust is given by the following equation.

$$f_x = \overline{f}_x + K_p\omega_p \tag{6}$$

$$f_y = \overline{f}_y - K_r\omega_r \tag{7}$$

$$m_z = \overline{m}_z - K_y\omega_y \tag{8}$$

where $\overline{f}_x$, $\overline{f}_y$, and $\overline{m}_z$ are the commanded thrust of the robot as described below, and K_p, K_r, and K_y are the feedback gains for sway suppression.

III. PATH FOLLOWING CONTROL

A. SLAM

In this study, LIO-SAM [12] in robot operating system (ROS) [13] package was used for SLAM. Preliminary experiments were conducted on the outdoor ground to investigate the accuracy of localization using LIO-SAM. The results showed that the LIO-SAM position estimation was in good agreement with the actual movement path and GNSS position measurement.

Since i-Boat2 is designed to navigate in port facilities, it is expected to navigate in places where the operator cannot see. Therefore, the positions of the robot, start and target points in autonomous navigation are visualized based on SLAM by LIO-SAM to ensure safe navigation. An environment where there is nothing around. In other words, SLAM may fail

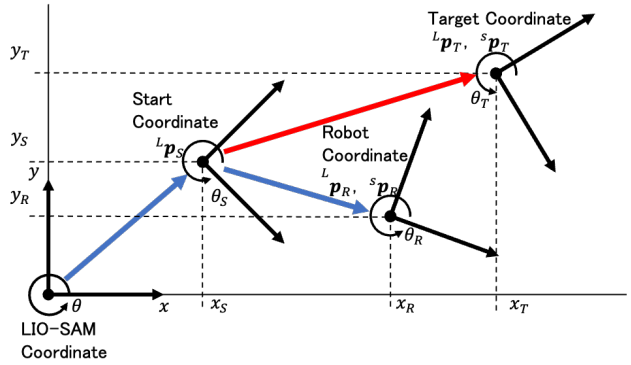

Fig. 5. Coordinate system of robot

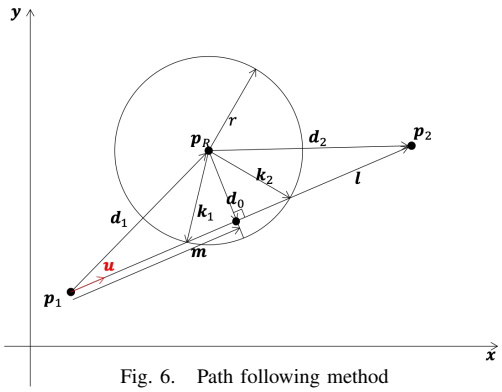

Fig. 6. Path following method

when completely offshore. However, it is effective for the purpose of surveying port facilities.

The coordinate system of LIO-SAM uses the coordinates at the time of program start as the origin and thus differs from the coordinate system that represents the start and target points of autonomous navigation. The relationship between the coordinate systems is shown in Fig. 5. Consider an absolute coordinate system (called the LIO-SAM coordinate system, denoted by superscript ^{L} in the upper left corner of the symbol) with the start point at the position where the SLAM program was started in the lower left corner. The point at which i-Boat2 moves and begins autonomous navigation is called the start coordinate system (denoted by superscript ^{S}). In autonomous navigation, i-Boat2 moves toward a predetermined target point in the start coordinate system.

Therefore, in order for i-Boat2 to know its current position (in the start coordinate system) with the autonomous navigation start position as the origin, the robot position ${}^{L}\boldsymbol{p}_R = {}^{L}[x_R,\ y_R,\ \theta_R]^{\mathrm{T}}$ in the LIO-SAM coordinate system should be converted to the robot position ${}^{S}\boldsymbol{p}_R = {}^{S}[x_R,\ y_R,\ \theta_R]^{\mathrm{T}}$ in the start coordinate system. If the rotation matrix around the Z-axis of the start coordinate system in the LIO-SAM coordinate system is ${}^{L}\boldsymbol{R}(\theta_S)$, the position of i-Boat2 in the LIO-SAM coordinate system are expressed by the following equation.

$$ {}^{L}\boldsymbol{p}_R = {}^{L}\boldsymbol{p}_S + {}^{L}\boldsymbol{R}(\theta_S)\,{}^{S}\boldsymbol{p}_R \tag{9} $$

Transforming this equation, ${}^{S}\boldsymbol{p}_R$ is obtained as follows:

$$ {}^{S}\boldsymbol{p}_R = {}^{L}\boldsymbol{R}(-\theta_S)\left({}^{L}\boldsymbol{p}_R - {}^{L}\boldsymbol{p}_S\right) \tag{10} $$

Similarly, if ${}^{S}\boldsymbol{p}_T = [x_T,\ y_T,\ \theta_T]^{\mathrm{T}}$ is the target point in the start coordinate system and ${}^{L}\boldsymbol{p}_T = [x_T,\ y_T,\ \theta_T]^{\mathrm{T}}$ is the target point in the LIO-SAM coordinate system, the following relation is given.

$$ {}^{L}\boldsymbol{p}_T = {}^{L}\boldsymbol{p}_S + {}^{L}\boldsymbol{R}(\theta_S)\,{}^{S}\boldsymbol{p}_T \tag{11} $$

B. Path Following

In a real wave environment, waves come from many different directions that are difficult to predict. Therefore, it is difficult to simply specify a destination point that is far away and then go straight to that point. Therefore, we consider a path following method that makes the robot follow the path from point 1 to point 2, which is represented by a straight line. Pure pursuit [14] is well known as a path following algorithm for two-wheeled robots. However, i-Boat2 can move in all directions, so the following algorithm is newly proposed.

Figure 6 is used to explain how to follow the path when the robot is a certain distance away from the path. Note that the absolute coordinate system is used here, and the superscript in the left corner is omitted. Let $\boldsymbol{p}_1$ be the position of start point 1 and $\boldsymbol{p}_2$ the position of end point 2 of the path (line segment) to be followed. Denoting the current position of the robot by $\boldsymbol{p}_R$, the vector $\boldsymbol{d}_1$ from start point 1 to the robot is given by

$$ \boldsymbol{d}_1 = \boldsymbol{p}_R - \boldsymbol{p}_1 \tag{12} $$

Also, the vector $\boldsymbol{l}$ from start point 1 to end point 2 is

$$ \boldsymbol{l} = \boldsymbol{p}_2 - \boldsymbol{p}_1 \tag{13} $$

The vector to the nearest neighbor point on the line $\boldsymbol{m}$ is shown by the following equation.

$$ \boldsymbol{m} = n\,\boldsymbol{u} \tag{14} $$

$$ n = \boldsymbol{u}^{\mathrm{T}}\,\boldsymbol{d}_1 \tag{15} $$

$$ \boldsymbol{u} = \boldsymbol{l}/\|\boldsymbol{l}\| \tag{16} $$

where n is the distance from the start point to the nearest neighbor and $\boldsymbol{u}$ is the unit vector from $\boldsymbol{p}_1$ to $\boldsymbol{p}_2$. If $n < 0$, the direction is the opposite of the direction from the start point to the end point. That the vector from the robot to the nearest neighbor point $\boldsymbol{d}_0$ can be obtained as follows.

$$ \boldsymbol{d}_0 = \boldsymbol{m} - \boldsymbol{d}_1 \tag{17} $$

Consider a path correction circle with radius r centered at robot position $\boldsymbol{p}_R$. If the robot is so far away that there is no intersection between the path correction circle and the path, or if there is only one intersection, i.e. $\|\boldsymbol{d}_0\| \geq r$, the robot is given a command thrust (in the direction of $\boldsymbol{d}_0$) towards the nearest neighbor point. If the path correction circle and the path have two intersections, i.e. $\|\boldsymbol{d}_0\| < r$, the command thrust (in the direction of $\boldsymbol{k}_2$) is given towards the intersection near point $\boldsymbol{p}_2$.

$$ \boldsymbol{k}_2 = \boldsymbol{d}_0 + \sqrt{r^2 - \|\boldsymbol{d}_0\|^2}\,\boldsymbol{u} \tag{18} $$

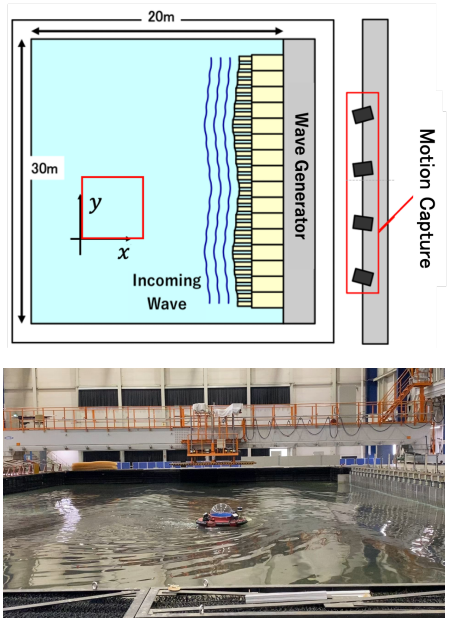

Fig. 7. Indoor experimental environment

If the end point $\boldsymbol{p}_2$ is included in the path correction circle, the command thrust (in the direction of $\boldsymbol{d}_2$) is given towards the end point.

$$\boldsymbol{d}_2 = \boldsymbol{p}_2 - \boldsymbol{p}_R \tag{19}$$

Including other detailed conditions and the coordinate transformation from the absolute coordinate system to the robot coordinate system, the final commanded thrust of the robot is given by the following equation.

$$\overline{\boldsymbol{f}}_R = [\overline{f}_x, \overline{f}_y]^{\mathrm{T}} \tag{20}$$

$$= {K_P}^L\boldsymbol{R}^{\mathrm{T}}(\theta_R)\boldsymbol{d} - {K_D}^L\boldsymbol{R}^{\mathrm{T}}(\theta_R)^L\dot{\boldsymbol{p}}_R \tag{21}$$

$$\boldsymbol{d} = \begin{cases} -\boldsymbol{d}_1 & \text{if } \|\boldsymbol{d}_1\| \geq r \text{ and } n < 0 \\ \boldsymbol{d}_2 & \text{if } \|\boldsymbol{d}_2\| < r \text{ or } n > \|\boldsymbol{l}\| \\ \boldsymbol{d}_0 & \text{if } \|\boldsymbol{d}_0\| \geq r \\ \boldsymbol{k}_2 & \text{otherwise} \end{cases} \tag{22}$$

$$\overline{m}_z = K_\theta(\theta_d - \theta_R) \tag{23}$$

where K_P and K_D are the proportional and derivative gains for position, K_θ is the proportional gain for angle (orientation), and θ_d is the target for angle (orientation).

IV. Indoor Experiments

The indoor experiments were conducted in an indoor pool equipped with a wave generator and a motion capture system, as shown in Fig. 7. The results of position estimation by SLAM are compared with the results of position measurement by motion capture.

A. Sway Suppression

As a preliminary experiment before the autonomous navigation experiment, the convergence of the sway of i-Boat2 around the roll and pitch was compared when the body was pushed by hand with and without sway suppression control. The results are shown in Fig. 8 and Fig. 9. The black line shows the results with sway suppression control and the gray line shows the results without sway suppression control. The applied force was not exactly the same because the human was pushing, but you can see that the sway is reduced faster with sway suppression control.

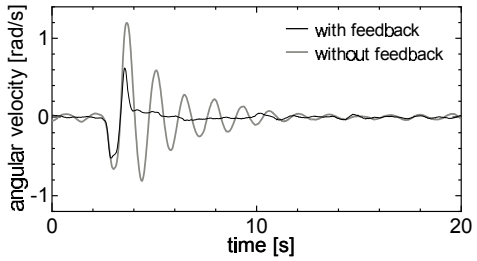

Fig. 8. Comparison of angular velocity around roll axis

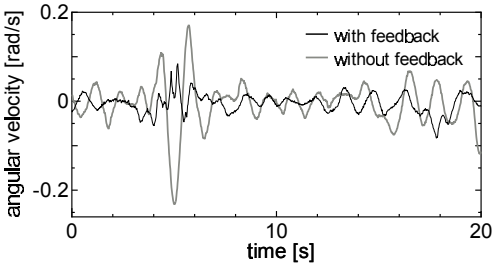

Fig. 9. Comparison of angular velocity around pitch axis

TABLE II
Experimental Conditions

case	wave height [cm]	period [s]	sway suppression	path following
1-0	–	–	w/o	w/o
1-1	10	1.0	w/o	w/o
1-2	10	2.0	w/o	w/o
1-3	10	3.0	w/o	w/o
1-4	10	4.0	w/o	w/o
1-5	30	2.0	w/o	w/o
1-6	30	3.0	w/o	w/o
2-0	–	–	with	w/o
2-1	10	1.0	with	w/o
2-2	10	2.0	with	w/o
2-3	10	3.0	with	w/o
2-4	10	4.0	with	w/o
2-5	30	2.0	with	w/o
2-6	30	3.0	with	w/o
3-0	–	–	with	with
3-1	30	2.0	with	with
3-2	30	3.0	with	with

B. Autonomous Navigation

Autonomous navigation experiments were conducted in which the vehicle circumnavigated a 5-meter square path. The experimental conditions are shown in Table. II. A total of 17 patterns were tested under four different conditions: wave height, wave period, with and without sway suppression control, and with and without path following control. The result for the case without sway suppression and path following (case 1-1) is shown in Fig. 10. Although the SLAM trajectory (red) deviates from the green path due to the lack of path following control, it can be seen that the SLAM trajectory passes close to the four target corners indicated

by the black dots. However, the motion capture trajectory (blue) has large deviations from the SLAM trajectory. This is due to the fact that SLAM's position estimation has been shifted by the shaking caused by the waves.

The results of case 2-1, where the sway suppression control was added, are shown in Fig. 11. The motion capture trajectory and the SLAM trajectory were almost identical, and the trajectory was close to the target path, confirming the effectiveness of the sway suppression control. i-Boat2 was able to estimate its own position even on waves, and although there were deviations in the paths between target points, it was confirmed that it was able to reach the target point.

Next, an example of the experimental results (case 3-1) with the path following control is shown in Fig. 12. The i-Boat2 with path following control reduces the deviation from the green straight line path even in waves, confirming that the i-Boat2 is able to navigate with greater stability.

V. Experiments at Sea

We have verified whether autonomous navigation is possible in a real wave environment using i-Boat2. Fig. 13 shows the experimental environment at the Nagoya Port, Japan. In the figure, the target path ① is a 5-meter square in the open sea, as in the indoor experiment. The target path ② is a 15-meter straight line that passes under the pier. Transit (TS) and GNSS (non-RTK and RTK) were also used for position measurement. An example of the experimental results with sway suppression control and without path following control for the path ① is shown in Fig. 14. Since each measurement system was used separately, the display positions are adjusted in the figure. The position information (scale and shape) from SLAM, TS, GNSS (non-RTK) and Ichimill (RTK-GNSS) were generally in agreement, indicating that SLAM's position estimation was fully functional. However, the trajectory resulted in a significant deviation from the straight line between the target points. In the absence of path following control, this may be due to the effects of large waves and currents in the natural ocean environment.

Next, Fig. 15 shows an example of the experimental results with path following control using the same 5-meter square path. It was confirmed that the orbit error was within 0.5 m, indicating the effectiveness of the path following control even at sea. Finally, Fig. 16 shows an example of the results of a round trip experiment with a straight path of 15 m passing under a pier. It can be confirmed that the robot was able to make a round trip along the straight path. However, the position information from GNSS (non-RTK) and Ichimill (RTK-GNSS) was corrupted. This is due to the fact that the satellite signals did not directly reach the area under the facility. It is believed that GNSS can be used for position measurement and control in the open sea, but again it is clear that there are limitations to its use under the facility.

VI. Conclusions

In this study, USV "i-Boat2" equipped with 3D LiDAR and IMU was developed for efficient inspection of port facilities. In an indoor pool with a wave generator, we confirmed that sway suppression control is effective in stabilizing SLAM position estimation even in the presence of waves, and demonstrated autonomous navigation within 0.5 m error using the path following method. We also verified the autonomous navigation experiment in real sea conditions.

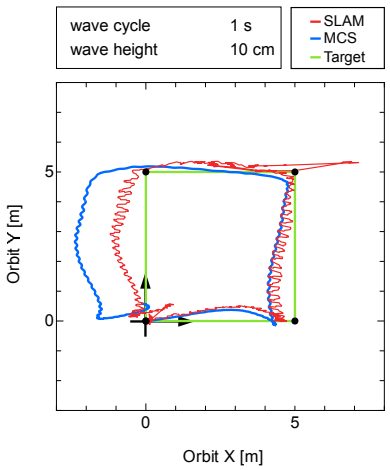

Fig. 10. Experimental result in case of 1-1

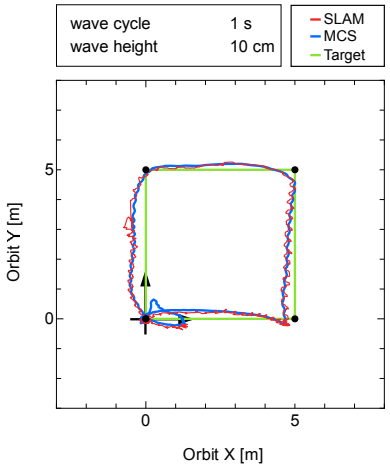

Fig. 11. Experimental result in case of 2-1

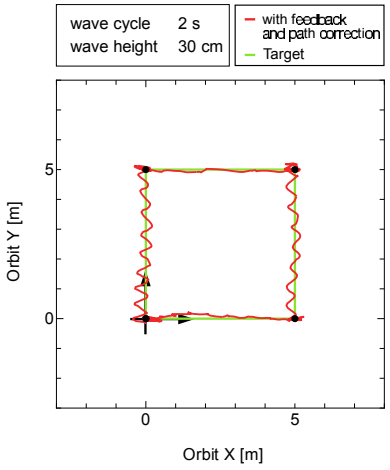

Fig. 12. Experimental result in case of 3-1

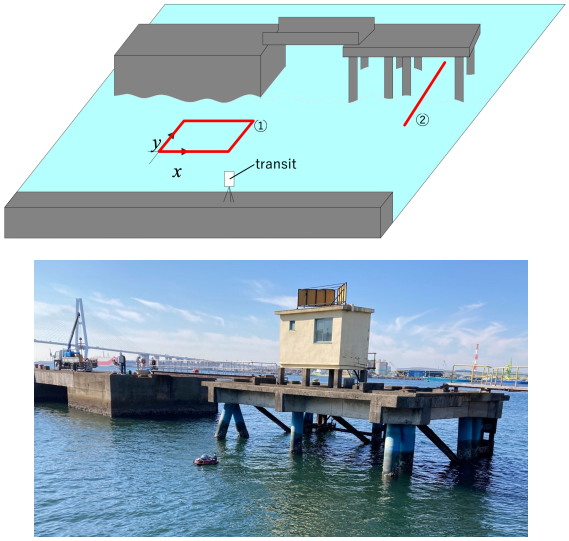

Fig. 13. Outdoor experimental environment

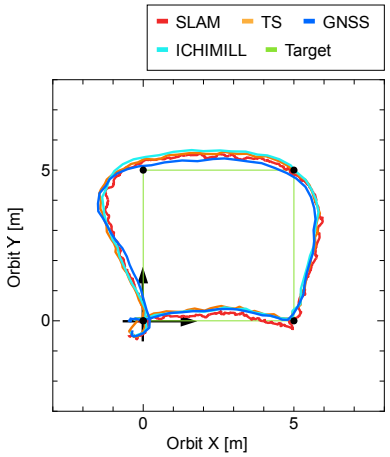

Fig. 14. Experimental result without path following control at sea with open sky

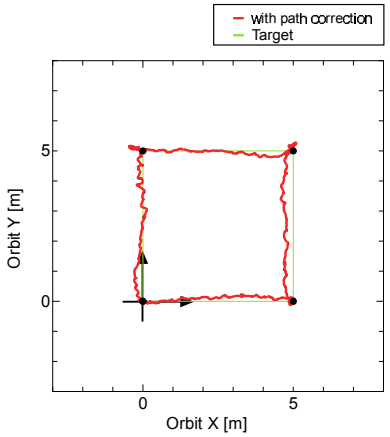

Fig. 15. Experimental result with path following control at sea

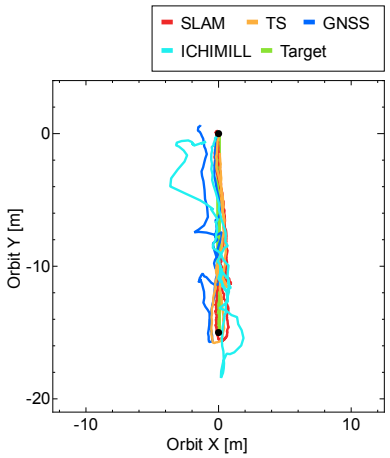

Fig. 16. Experimental result passing under pier

REFERENCES

[1] Ministry of Land, Infrastructure, Transport and Tourism (MLIT), Ports and Airports Research Institute (PARI), and Ocean Policy Research Foundation (OPRF), *Guidelines on Strategic Maintenance for Port Structures*. MLIT, 2011.

[2] K. Mizuno, T. Sakai, T. Ogasawara, H. Sugimoto, and S. Motoyama, "Development of inspection and diagnosis system on the lower side of the pier using a radio control boat," *Journal of Japan Society of Civil Engineers, Ser. B3 (Ocean Engineering)*, vol. 73, no. 2, pp. I_432–I_437, 2017, (in Japanese).

[3] K. Mizuno, "System of Inspection and Diagnosis for Port Structures Using Unmanned Boat," Penta-Ocean Construction Co., Ltd., Tech. Rep., 2019.

[4] O. Yaakob, Z. Mohamed, M. Hanafiah, D. Suprayogi, M. Abdul Ghani, F. Adnan, M. Mukti, and J. Din, "Development of unmanned surface vehicle (USV) for sea patrol and environmental monitoring," in *Proceedings of the International Conference on Marine Technology, Kuala Terengganu, Malaysia*, 2012, pp. 20–22.

[5] J. Villa, J. Aaltonen, and K. T. Koskinen, "Path-following with lidar-based obstacle avoidance of an unmanned surface vehicle in harbor conditions," *IEEE/ASME Transactions on Mechatronics*, vol. 25, no. 4, pp. 1812–1820, 2020.

[6] N. Wang and X. Pan, "Path following of autonomous underactuated ships: A translation–rotation cascade control approach," *IEEE/ASME Transactions on Mechatronics*, vol. 24, no. 6, pp. 2583–2593, Dec 2019.

[7] J. Han, J. Han, Y.-H. Cho, Y.-H. Cho, J. Kim, J. Kim, J. Kim, J. Kim, N.-S. Son, N. sun Son, S. Y. Kim, and S. Y. Kim, "Autonomous collision detection and avoidance for aragon usv: Development and field tests," *Journal of Field Robotics*, 2020.

[8] Z. Liu, Y. Zhang, X. Yu, and C. Yuan, "Unmanned surface vehicles: An overview of developments and challenges," *Annual Reviews in Control*, vol. 41, pp. 71–93, 2016.

[9] M. MINAMI, "Current status and issues of underwater drone," *Journal of The Society of Instrument and Control Engineers*, vol. 59, no. 7, pp. 492–496, 2020.

[10] S. Shimono and S. Shimono, "Evaluation of under water positioning by hanged rov from usv," *International Journal of Modeling and Optimization*, 2017.

[11] K. Xue, X. Ji, D. Qu, Y. Peng, and H. Qian, "OBoat: An Agile Omnidirectional Robotic Platform for Unmanned Surface Vehicle Tasks," *IEEE/ASME Transactions on Mechatronics*, vol. 28, no. 5, pp. 2413–2424, 2023.

[12] T. Shan, B. Englot, D. Meyers, W. Wang, C. Ratti, and D. Rus, "LIO-SAM: Tightly-coupled Lidar Inertial Odometry via Smoothing and Mapping," in *2020 IEEE/RSJ International Conference on Intelligent Robots and Systems (IROS)*, 2020, pp. 5135–5142.

[13] M. Quigley, K. Conley, B. P. Gerkey, J. Faust, T. Foote, J. Leibs, R. Wheeler, and A. Y. Ng, "ROS: An open-source robot operating system," in *Workshops at the IEEE International Conference on Robotics and Automation*, 2009.

[14] R. C. Coulter, "Implementation of the pure pursuit path tracking algorithm," Pittsburgh, PA, Tech. Rep. CMU-RI-TR-92-01, January 1992.